REMOVAL OF TETRACYCLINE FROM AQUEOUS SOLUTIONS USING NANOSCALE ZERO VALENT IRON AND FUNCTIONAL PUMICE MODIFIED NANOSCALE ZERO VALENT IRON

Ulker Asli GULER

Department of Environmental Engineering, Engineering Faculty, Cumhuriyet University, Sivas, Turkey

Abstract. Nanoscale zero valent iron (nZVI) and functional pumice modified nanoscale zero valent iron (P-nZVI) were successfully synthesized and used for the removal of tetracycline (TC). These materials were characterized by SEM, TEM, XRD, FTIR, BET. Different factors such as the mass ratio, dosage of adsorbent, pH, initial TC concentration and temperature were investigated. Based on these results; a possible removal mechanism was proposed including TC adsorption and TC reduction via oxidation of Fe^0 to Fe^{3+}. In addition, isotherm and thermodynamic parameters were applied to the equilibrium data. The maximum adsorption capacity of TC by nZVI and P-nZVI was 105.46 mg/g and 115.13 mg/g, respectively. Adsorption and reduction kinetics were examined for the TC removal process. The pseudo-second-order model and pseudo-first-order model was observed for adsorption and reduction process, respectively. Finally, more than 90% of TC from aqueous solutions was removed by nZVI and P-nZVI.

Keywords: tetracyline, antibiotic, characterization, pumice, nanoscale zero valent iron, removal, batch.

Introduction

Tetracylines (TCs) have been widely used in human therapy and the livestock industry (Zhao *et al.* 2011). TCs are poorly adsorbed in metabolizm. 30–50% of the initial TCs amount could be absorbed by digestive tract of humans and animals (Song *et al.* 2014). Residues of TCs were excreted to the environment via different pathways such as direct discharge of agriculture products and the excretion of substances in livestock urine and feces (Zhao *et al.* 2011; Boxall 2003). Although *TC* concentrations and their byproducts were low in the environment, they may lead to development of antibiotic resistant microbial populations as well as environmental and human health problems (Zhao *et al.* 2011; Daughton, Ternes 1999).

The *TC* molecule has three multiple ionisable functional groups: a tricarbonylamide group (C-1-C-3), a dimethylammonium group (C-4) and a phenolic diketone group (C-10-C-12) and is amphoteric (Fig. 1) (Zhao *et al.* 2012; Li *et al.* 2010; Chen *et al.* 2011). They can undergo protonation-deprotonation reactions and present different ionic species depending on the solution pH (Zhao *et al.* 2011). *TC* species are a cation (H_3TC^+, pH< 3.3), neutral (H_2TC^0, 3.3 < pH < 7.70), an anion (HTC^-, 7.70 < pH < 9.70) or two anion (TC^{2-}, pH > 9.70) (Zhao *et al.* 2012).

Previous studies show that the principal removal mechanism of *TC* was adsorption process. Natural and nano materials such as goethite (Zhao *et al.* 2012), activated sludge (Song *et al.* 2014), kaolinite (Li *et al.* 2010), clay minerals (Chang *et al.* 2009a), illite (Chang *et al.* 2012), and magnetite nanoparticles (Zhang *et al.* 2011a) have
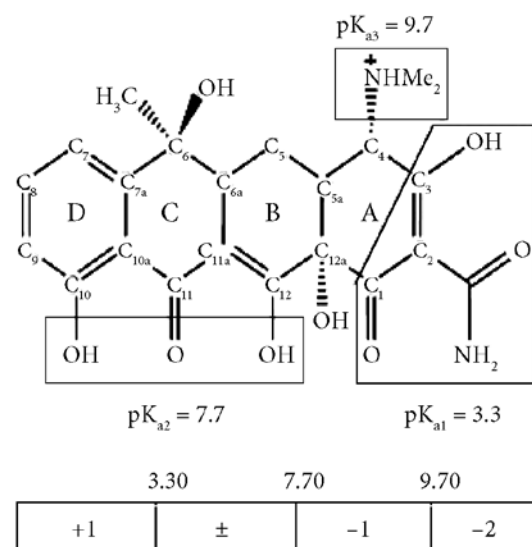
Fig. 1. Structure of TC

Corresponding author: Ulker Asli Guler
E-mail: ulkerasli@gmail.com

Taylor & Francis
Taylor & Francis Group

been used in previous studies. Recently, nZVI in powder or granular form has been used to remove pollutants such as heavy metals, chlorinated organic, dyes, pharmaceutical compounds (Fang *et al.* 2011; Dickinson, Scott 2010; Kim *et al.* 2013; Li *et al.* 2012; Chen *et al.* 2013). This is because of its extremely small particle size, large specific surface area, high density, effective and high reactivity (Üzüm *et al.* 2009; Cao, Zhang 2006; Kanel *et al.* 2006). Based on these characteristics, nZVI technology could become a promising approach for treating antibiotic wastewater. However, nZVI has usually been agglomerated in conventional systems along with a decrease in its reactivity and mechanical strength, which have limited its practical applications (Liu *et al.* 2014; Cumbal *et al.* 2003). Recently, porous materials such as zeolite (Kim *et al.* 2013), kaolinite (Üzüm *et al.* 2009), pillared bentonite (Li *et al.* 2012) and pillared clay (Zhang *et al.* 2011b) have been widely used as mechanical supports to enhance the dispersibility of nZVI particles. All of these studies suggest that the use of supported nZVI is promising for the remediation of contaminated sites (Li *et al.* 2012). However, some immobilization methods are quite complex, so the development of more efficient immobilization systems is required for practical applications (Li *et al.* 2012).

Pumice is a light, porous volcanic rock and has a large surface area and skeleton structure (Asgari *et al.* 2012). Pumice is generally pale in color, ranging from white, cream, blue or grey to greenish-brown or black (Guler, Sarioglu 2014). Pumice has been used in water treatment as a low-cost adsorbent, filter and support media (Fang *et al.* 2011; Liu *et al.* 2014; Kitis *et al.* 2007). Only a few heavy metal removal studies have used pumice with nZVI (Liu *et al.* 2014; Moraci, Calabro 2010). For these reasons, this study focused on removal of *TC* onto functional pumice modified nanoscale zero valent iron (P-nZVI). The aim of this study was to understand the removal of *TC* antibiotic compounds from wastewaters using nZVI and P-nZVI. The synthesis of the stable nZVI and P-nZVI composites, characterization, effect of various parameters on the removal process, kinetic studies of the adsorption and reduction process; adsorption isotherms and thermodynamic parameters, and possible removal mechanisms are reported in this study.

1. Materials and methods

1.1. Materials and chemicals

Pumice was provided by Kayseri-Basakpınar in Turkey and the chemical composition was 69.27% SiO_2, 22.1% Al_2O_3, 3.89% K_2O, 3.61% Na_2O, 2.90% Fe_2O_3, 1.82% CaO and small amounts of Mg, Ti, S, P, Mn, Ba, Zr, Cr and Zn. After washing with distilled water, it was oven dried at 50 °C. Later, the particle size of dried pumice stone was

ground particles smaller than 0.125 mm. Iron (II) chloride tetrahydrate ($FeCl_2·4H_2O$), sodium borohydride ($NaBH_4$) and ethanol were supplied by Sigma Aldrich. *TC* was provided by a pharmaceutical factory in Turkey. All chemicals were of analytical grade purity.

1.2. Preparation of nZVI and P-nZVI

nZVI and P-nZVI were synthesized using borohydride reduction method (Üzüm *et al.* 2009). $FeCl_2·4H_2O$ and sodiumborohydride ($NaBH_4$) were used and pumice was used as a support material [16]. Briefly, the preparation of P-nZVI composites had pumice to nZVI mass ratio of 1:1, 1:2 and 2:1. For the 1:1; $FeCl_2·4H_2O$ (5.34 g) was dissolved in ethanol and water mixture (30 mL; 4:1 v/v), then 1.5 g of pumice was added to this solution and stirred for 30 min. Meanwhile, a prepared 1.0 M $NaBH_4$ solution (3.05 g $NaBH_4$ in 100 mL of deionized water) was added dropwise into the pumice-Fe^{2+} mixture on the magnetic stirrer. Black solid particles of nZVI appeared immediately after the first drop of $NaBH_4$ solution was added. After adding all of the borohydride solution, the mixture was left stirring for an additional 10 min. The reduction of iron ions by borohydride ions can be represented by the following reaction (Wang *et al.* 2006):

$$>Fe^{2+} + 2BH^-_{4(aq)} + 6H_2O \rightarrow Fe^0 + 2B(OH)_3 + 7H_2\uparrow. \qquad (1)$$
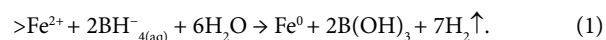
The synthesized materials were separated from the liquid phase via the vacuum filtration. Solid particles were washed with absolute ethanol. The synthesized material was oven dried at 50 °C. The pumice:nZVI mass ratios (1:2 and 2:1) were synthesized following the same method. nZVI and P-nZVI composites were stored in brown bottles for later use.

1.3. Experiments with different pumice to nZVI mass ratios

0.05 g of P-nZVI prepared by different mass ratios of pumice to nZVI (1:1, 1:2 and 2:1) was added into 100 mL of 50 mg/L *TC* solutions. Solution pH values were adjusted to 4.00 by ADWA pH meter. The Erlenmeyer were shaken in a shaker at 200 rpm for 60 min. After centrifugation, the supernatant solutions were analyzed with a spectrophotometer (CHEBIOS) at 357 nm wavelength.

1.4. Batch experiments

Batch experiments were performed in Erlenmeyer with 100 mL of aqueous solution. Effect of nZVI and P-nZVI amounts (2:1) (2–10 g/L), solution pH (2–10), initial *TC* concentration (25–300 mg/L) and temperature (25–45 °C) on *TC* removal using nZVI and P-nZVI was investigated. The solutions were shaken in a temperature controlled shaker (GERHARD) at 150 rpm. Sampling was made at a certain time-interval (5–180 min) and then

the supernatant solutions were transferred to falcon tubes. The samples were centrifuged by centrifugation (Hettich EBA 21). All experiments were performed in duplicate. The details of the experimental conditions are presented in Table 1.

1.5. Characterization and analytical methods

The adsorption capacity (q_e, mg/g) is given below (Guler, Sarioglu 2014):

$$q_e = \frac{\left(\left[TC\right]_o - \left[TC\right]_e\right)V}{m}, \qquad (2)$$

where $\left[TC\right]_o$ and $\left[TC\right]_e$ are the initial and the equilibrium concentration (mg/L), V is the volume of solution (L) and m is the amount of nZVI and P-nZVI (g).

The removal efficiency of *TC* (%) is described as follows (Guler, Sarioglu 2014):

$$Sorption\,(\%) = \frac{\left[TC\right]_o - \left[TC\right]_e}{\left[TC\right]_o} \times 100. \qquad (3)$$

The nZVI and P-nZVI samples were collected after reacting with *TC* solution for 5, 10, 15, 30, 60, 120 and 180 min. Morphological analyses were performed using a scanning electron microscope (SEM) (LEO, 440) and transmission electron microscope (TEM) (JEOL JEM 1220). All TEM samples were prepared from depositing a drop of dilute ethanol solution of the nanoparticles onto a carbon film. The chemical bonds between the atoms and the functional groups of material were identified by FTIR method. The FTIR samples in KBr pellets were analyzed by a Perkin Elmer Spectrum 400 spectrometer. The crystalline phases of nZVI and P-nZVI were determined by used XRD diffractometer. A Cu Kα incident beam (λ = 1.54 nm) was used (Bruker AXS D8 Advance). The specific surface area (BET) was measured following the Brunauer-Emmett-Teller (BET) N_2 method.

2. Results and discussion

2.1. Characterization of materials

The FTIR spectrum of the nZVI and P-nZVI composites before and after *TC* removal are shown in Figure 2. Broads bands at 3200–3600 cm^{-1} may have resulted from O-H stretching. O-H bending was observed at the 1645 cm^{-1} band. Bands at <900 cm^{-1} in the nZVI may be related with iron oxides. These bands in the P-nZVI are weaker due to reduced oxidation of pumice modified Fe^0. According to Kim *et al.* (2013), the pumice support may reduced Fe hydroxide formation. Similar results were obtained from other studies (Kim *et al.* 2013; Yuan *et al.* 2009). Bands at 1336–1128 cm^{-1} resulted from ethanol used in preparing the composites. Composites may include bands associated with sulfate green rust and lepidocrocite formation on some Fe^0 surfaces (Kim *et al.* 2013; Andrade *et al.* 2009). The FT-IR spectra of TC-nZVI and TC-P-nZVI are different from those of nZVI and P-nZVI.

XRD spectrums of nZVI, TC-nZVI, P-nZVI, and TC-P-nZVI are presented in Figure 3. There were peaks at 22° and 28° in P-nZVI, which are associated with mineral dachiardite (Ca, Na, K, Al, Si and H_2O) (Guler, Sarioglu 2014; Ersoy *et al.* 2010). The apparent peak at 44.9° in nZVI and P-nZVI indicated that Fe^0 nanoparticles were modified onto the pumice surface (Chen *et al.* 2011; Fang *et al.* 2011; Zhang *et al.* 2011c). The peaks at 30° and 33° are related to $Fe_3O_4/\gamma-Fe_2O_3$ and FeO, respectively. These iron oxides also appeared in P-nZVI (Zhang *et al.* 2011c; Kanel *et al.* 2005).

The SEM images of nZVI (a), P-nZVI (b), TC-nZVI (c), and TC-P-nZVI (d) are shown in Figure 4. The nZVI and P-nZVI composites were aggregated from the van der Waals and magnetic forces (Kim *et al.* 2013; Wang *et al.* 2013). The SEM images after reaction showed that the external surfaces of nZVI and P-nZVI were covered by TC.

Table 1. Experimental conditions for adsorption studies

| Set | Aim of experiment | Experimental conditions | | | | | |
		Pumice:nZVI mass ratio	pH	*TC* conc. (mg/L)	Adsorbent amount (g/L)	Contact time (min)	Temperature
1	Pumice:nZVI mass ratio	1.1, 1:2, 2:1	4.0	50	5	60	25 °C
2	Effect of nZVI and P-nZVI amounts	2:1	4.0	50	2–5–10	5–10–15–30–60–120–180	25 °C
3	Effect of pH value	2:1	2–4–6–8–10	50	5	5–10–15–30–60–120–180	25 °C
4	Adsorption isotherms	2:1	8.0	25–50–100–200–300	5	5–10–15–30–60–120–180	25 °C
5	Adsorption kinetics	2:1	4.0	50	5	5–10–15–30–60–120–180	25 °C
6	Effect of temperature	2:1	8.0	50	5	5–10–15–30–60–120–180	25–35–45 °C
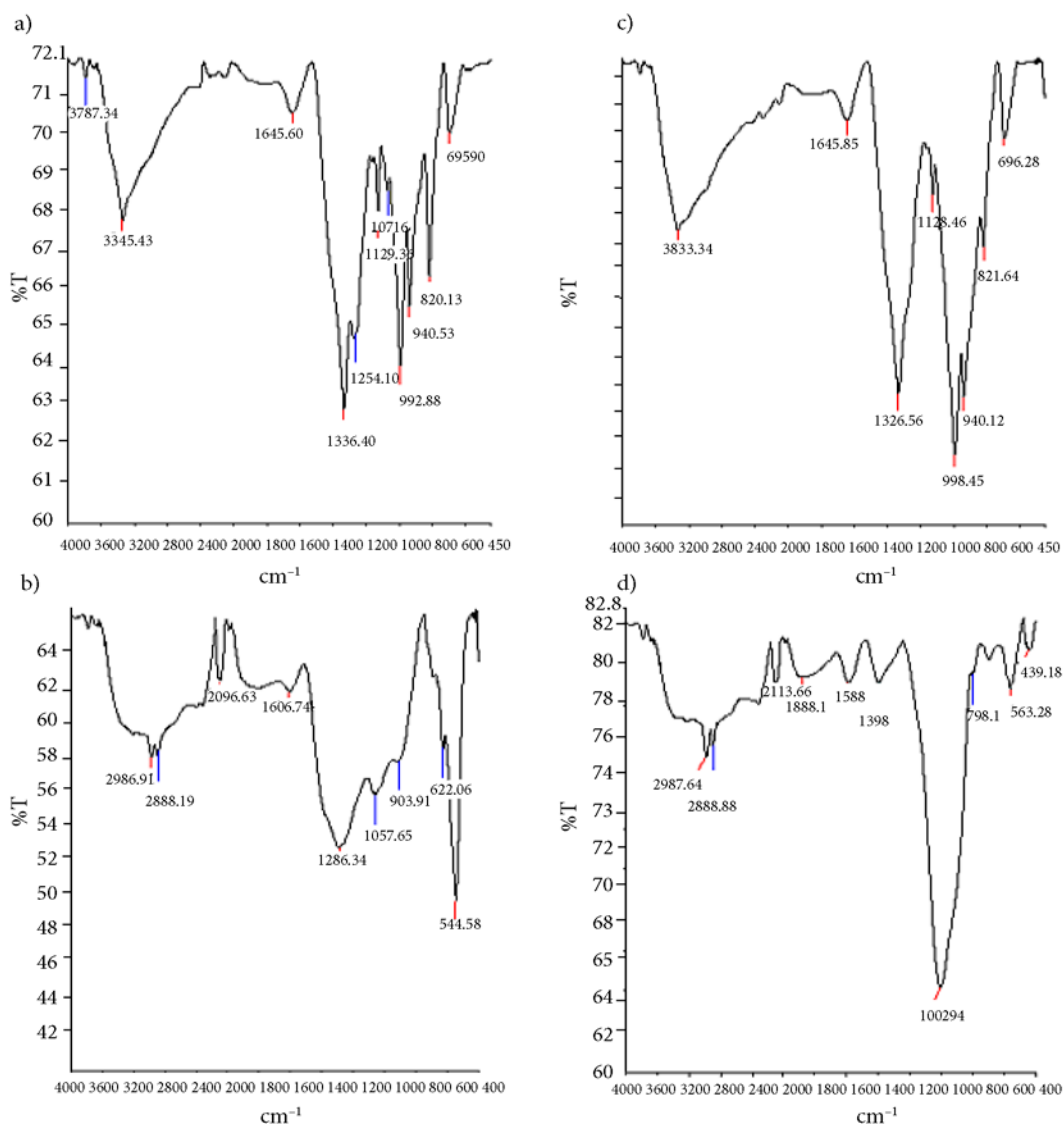
Fig. 2. FTIR patterns of nZVI (a), *TC*-nZVI (b), P-nZVI (c), and *TC*-P-nZVI (d)

In Figure 5 is presented TEM images of the nZVI and P-nZVI. The laboratory prepared nZVI and P-nZVI were spherical. TEM images also show that most particles formed chain-like aggregates (Sun *et al. 2006*). Aggregation of the nanoparticles is caused by the large surface area and magnetic dipole-dipole interactions of the particles. TEM analysis of a aged sample of nZVI showed that the chain-like structure was stil dominant but indicated also the presence of some larger floc aggregates, stemming possibly from the enhancement in oxide formation (Üzüm *et al.* 2008).

The BET surface area, total pore volume and mean pore size of nZVI and P-nZVI were 21.67 m^{2}g^{-1}, 0.10 cm^{3}g^{-1}, 40 nm and 12,41 m^{2}g^{-1}, 0.05 cm^{3}g^{-1}, 27 nm, respectively.

2.2. Parameters affecting *TC* removal

2.2.1. Pumice:nZVI mass ratio

Figure 6a showed that removal efficiency of *TC* increased the mass ratio as increased from 1:2 to 2:1. Using pumice

as support material for nZVI created a synergetic effect for the *TC* removal process (Kim *et al.* 2013). Similar trends were reported for nitrate (Zhang *et al.* 2011b), organic contaminants (Zhang *et al.* 2011d) and Cr(VI) removal (Li *et al.* 2012).

2.2.2. Effect of nZVI and P-nZVI amounts

The removal efficiency of *TC* varied with contact time, from 5 min to 180 min under with different amounts of nZVI and P-nZVI (Fig. 6b). Removal efficiency of *TC* increased with increasing nZVI and P-nZVI amount and contact time. The removal efficiency of *TC* increased from 67% to 77% and 37% to 52% by increasing amounts from 1 to 5 g/L of nZVI and P-nZVI amount, respectively. Figure 4b shows that 5 g/L nZVI and P-nZVI exhibited better removal efficiency than 1 g/L nZVI and P-nZVI. The removal efficiency of *TC* by nZVI was much higher than P-nZVI. These results may be explained with the more adsorptive and active surface sites (Chen *et al.* 2013). The
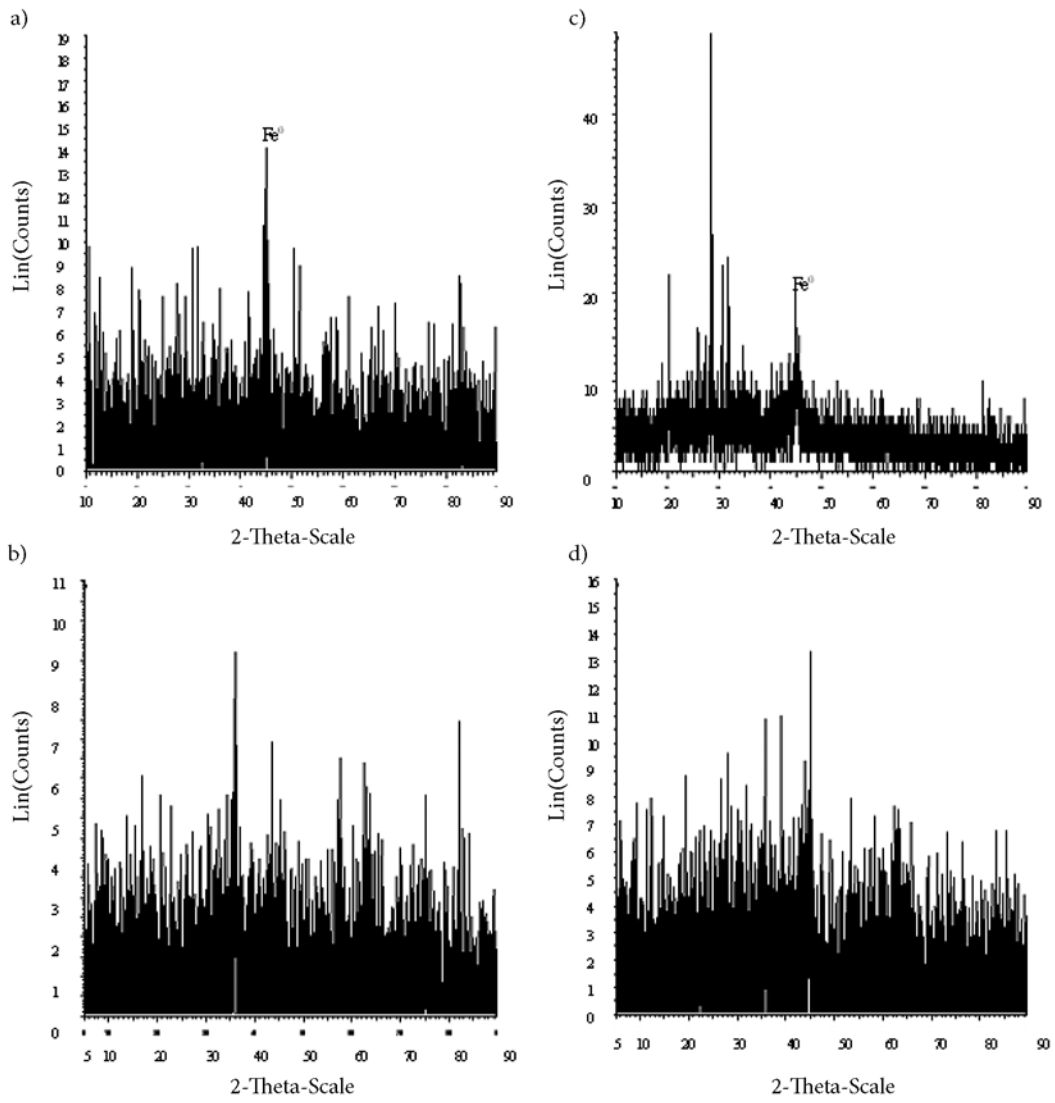
Fig. 3. XRD spectrums of nZVI (a), *TC*-nZVI (b), P-nZVI (c), and *TC*-P-nZVI (d)
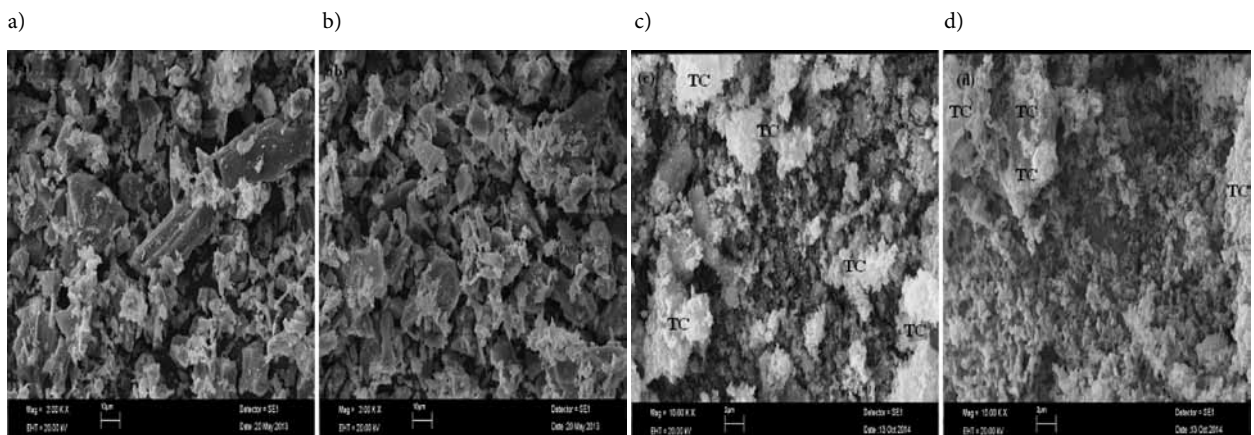
Fig. 4. SEM images of of nZVI (a), P-nZVI (b), *TC*-nZVI (c), and *TC*-P-nZVI (d)

optimum dosage of nZVI and P-nZVI was selected as 5 g/L which was used in further experiments.

2.2.3. Effect of pH value

The pH is an important factor affecting removal efficiency of *TC* by iron (Chen *et al.* 2011). The effect of pH on the *TC* removal rates and the zero point of charge (pH$_{pzc}$) are presented in Figure 6c. The effects of different initial solution pH (2–4–6–8–10) were studied using a 100 mL solution containing 50 mgTC/L with contact times of 5–10–15–30–60–120–180 min. pH$_{pzc}$ values of nZVI and P-nZVI were found to be approximately 9.30.

After 180 min at pH 2, 4 and 6, the average removal efficiency of *TC* was approximately 92% and 88% for nZVI and P-nZVI; at pH 8 and pH 10, it was approximately 88% and 72%, respectively. At pH < 3.3; 3.3 < pH < 7.7 and 7.70 < pH < 9.70, H_3TC^+ (cationic), H_2TC^0 (zwitterionic) and HTC^- (anionic) species of *TC* were dominant (Zhao *et al.* 2012; Chen *et al.* 2011). When pH was lower than the pH$_{PZC}$ of nZVI and P-nZVI, the composites surface was positively charged. The removal mechanism might be via surface complexation and/or cation exchange on the surface sites (Fang *et al.* 2011). When pH was greater the pH$_{PZC}$ of nZVI and P-nZVI, surfaces areas were negatively charged. In this situation, the decrease in removal efficiency may be explained by electrostatic repulsion between surface areas and *TC* molecules (Ersoy *et al.* 2010). At lower pH, corrosion of nZVI composite was accelerated and Fe^{3+}-TC hydroxides on the iron surface contributed to
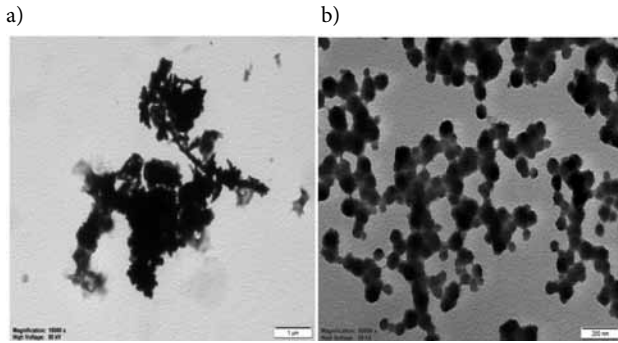
Fig. 5. TEM images of of nZVI (a), and P-nZVI (b)
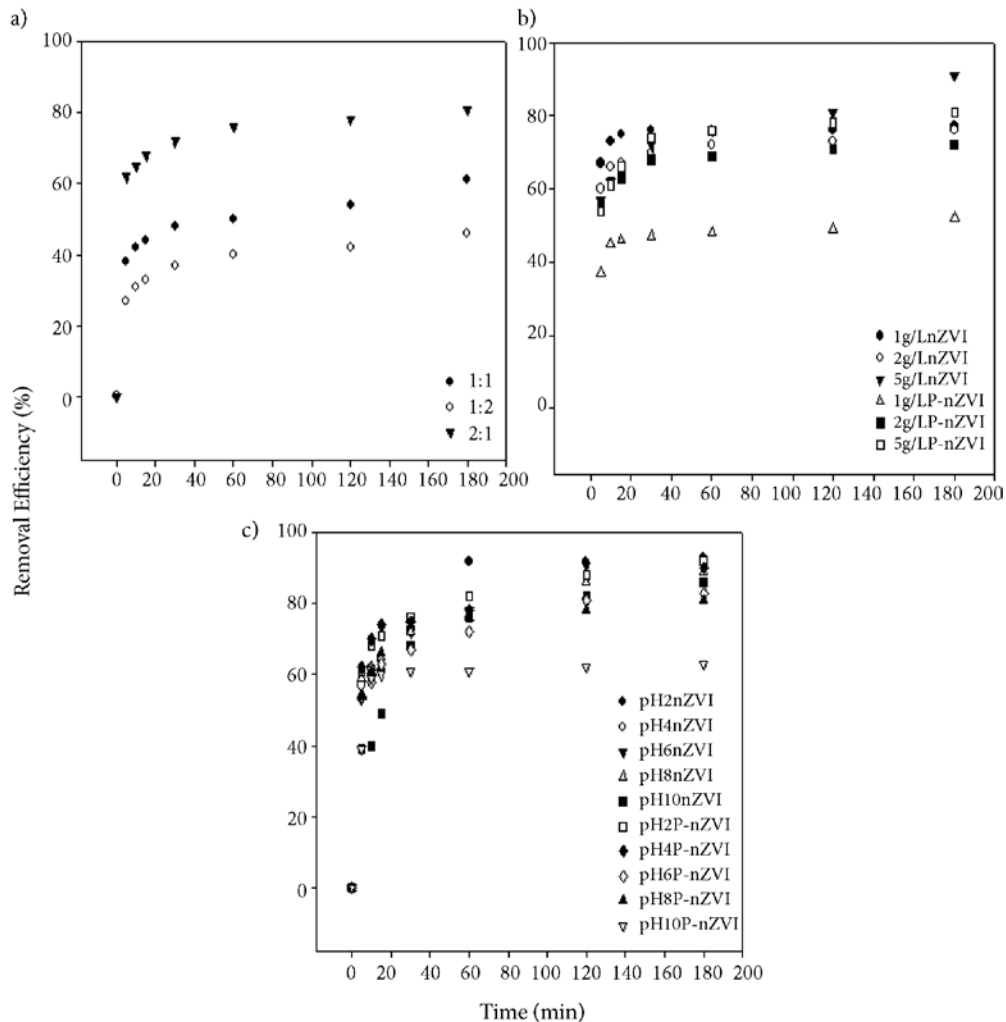
Fig. 6. Effect of different parameters on *TC* removal (a) mass ratios of pumice to nZVI (*Conditions*: 298 K, 200 rpm, 50 mgTC/L, pH$_{(initial)}$: 4.0, 5 g/L, 100 mL), (b) adsorbent amount and pH$_{PZC}$ (*Conditions*: 298 K, 200 rpm, 50 mgTC/L, pH$_{(initial)}$: 4.0, pumice:nZVI = 2:1, 100 mL), (c) solution pH (*Conditions*: 5 g/L, 298 K, 200 rpm, 50 mgTC/L, pumice:nZVI = 2:1, 100 mL)

the increase of *TC* removal (Li *et al.* 2012). Similarly, *TC* removal by P-nZVI decreased when initial pH increased. The reason for this condition may have an additional effect of functional groups on pumice. These results indicated that the *TC* removal using nZVI and P-nZVI can be studied over a wide pH range.

2.3. Adsorption isotherms

The equations of the Langmuir, Freundlich and D-R models are given below (Guler, Sarioglu 2014; Gao *et al.* 2012):

$$q_e = \frac{Q_m b [TC]_e}{1 + b[TC]_e} \; ; \tag{4}$$

$$q_e = k_F [TC]_e^{\frac{1}{n}} \; ; \tag{5}$$

$$q_e = q_{D-R} e^{\beta \varepsilon^2} \; ; \tag{6}$$

$$q_e = \frac{RT}{b_T} \ln(K_T [TC]_e) \; , \tag{7}$$

where, $[TC]_e$ (mg/L) indicates the equilibrium concentrations in aqueous phase after the adsorption of *TC* on nZVI and P-nZVI. q_e (mg/g) is the equilibrium adsorption capacity of nZVI and P-nZVI. Q_m (mg/g) and q_{D-R} (mol/g) are the maximum adsorption capacities, b (L/mg), k_F (L/g), and β

(mol²/J²) are the constant of Langmuir, Freundlich and D-R models, respectively. n and ε (J/mol) are the Freundlich linearity index and the Polanyi potential, respectively. The mean free energy *E* (kJ/mol) is expressed as below:

$$E = \frac{1}{\sqrt{2\beta}} \; . \tag{8}$$

Isotherm graphics are given in Figure 7 a, b and the isotherm parameters and correlation coefficients for *TC* are listed in Table 2.

As shown in Table 2, experimental data excellent fit both the Langmuir and Freundlich isotherm models (all exceed 0.960). Thus, the adsorption process occurred on a homogeneous adsorbent surfaces and on a reversible heterogeneous surfaces in the adsorption sites (Chen *et al.* 2013). The maximum adsorption capacity (Q_m) of *TC* for nZVI and P-nZVI was 105.46 mg/g and 115.13 mg/g, respectively. These values were much higher than adsorptions capacities of other adsorbents (Table 3) (Li *et al.* 2010; Chen *et al.* 2011; Xu, Li 2010; Chang *et al.* 2009b; Figueroa *et al.* 2004). P-nZVI had a much higher b (L/mg) (Langmuir constant) than nZVI, which verifies the advantageous *TC* adsorption of P-nZVI (Xu, Li 2010). The E value of adsorption was higher than 8 kJ/mol for all results, suggesting that the adsorption mechanism may be a chemisorption.
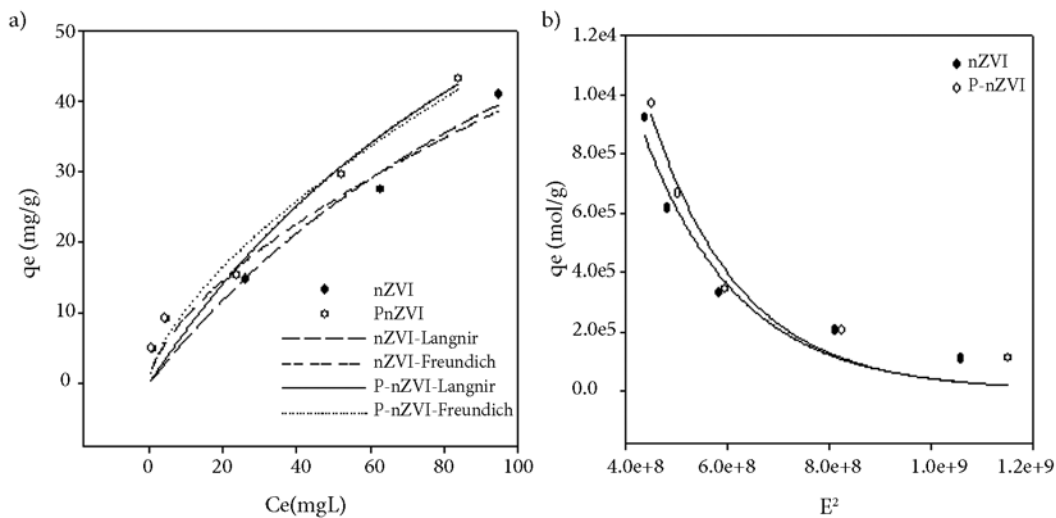
Fig. 7. Langmuir, Freundlich (a) and D-R (b) isotherm plots for adsorption of *TC* onto nZVI and P-nZVI

Table 2. Isotherm parameters and correlation coefficients of *TC* adsorption on nZVI and P-nZVI

nZVI									
Langmuir model			Freundlich model			D-R model			
Q_m (mg/g)	b (L/mg)	R^2	k_F (L/g)	$1/n$	R^2	q_{D-R} (mol/g)	E (kJ/mol)	β (mol²/J²)	R^2
105.46	0.0063	0.962	2.267	0.62	0.979	0.0009	9.63	$5.3978.10^{-9}$	0.970
P-nZVI									
Langmuir model			Freundlich model			D-R model			
Q_m (mg/g)	b (L/mg)	R^2	k_F (L/g)	$1/n$	R^2	q_{D-R} (mol/g)	E (kJ/mol)	β (mol²/J²)	R^2
115.13	0.0070	0.970	2.356	0.65	0.982	0.0012	9.38	$5.6889.10^{-9}$	0.975

Table 3. *TC* adsorption capacities using different adsorbents

Adsorbent	Q_m (mg/g)	Reference
nZVI	105.46	This study
P-nZVI	115.13	This study
Kaolinite	4.32	(Li *et al.* 2010)
Marine sediments	16.7–33.3	(Xu, Li 2010)
Palygorskite	61.8	(Chang *et al.* 2009b)
Montmorillonit	54	(Figueroa *et al.* 2004)

2.4. Kinetic studies

The *TC* removal on nZVI and P-nZVI was contained adsorption and reduction process.

2.4.1. Adsorption kinetics

The non-linear form of the pseudo-first order, pseudo-second order and intra particle models are applied to adsorption studies. These models depended on the physical and/or chemical properties of the adsorbent (Chen *et al.* 2013). The pseudo-first-order model is given below:

$$q_t = q_e(1 - e^{-k_1 t}),\qquad(9)$$

where q_e and q_t (mg/g) are the amounts of *TC* molecules adsorbed on the nZVI and P-nZVI at equilibrium and different time and k_1 (min^{-1}) is the rate constant of the pseudo-first-order model for the adsorption process.

The pseudo-second-order model can be shown as follows:

$$q_t = \frac{k_2 q_e^2 t}{1 + k_2 q_e t},\qquad(10)$$

where q_e and q_t (mg/g) are the amounts of *TC* molecules adsorbed on the nZVI and P-nZVI at equilibrium and different time and k_2 (g.mg^{-1}min^{-1}) is the rate constant of the pseudo-first-order model for the adsorption process.

Intraparticle model is given below:

$$qt = k_i t^{0.5} + C,\qquad(11)$$

where: k_i (mg/g·min$^{0.5}$) and C are the rate constant of intraparticle diffusion model and the intercept, respectively. The larger the intercept is the greater is the contribution of the surface sorption in the rate controlling step. The plots of qt *vs. t* for pseudo-first order and pseudo-second order kinetic model and the plot of qt *vs.* $t^{0.5}$ for intra particle model are presented in Figure 8a, b. The calculated coefficients and correlation coefficients are listed in Table 4.

According to the results, adsorption kinetics for all studies fit well with the pseudo-second-order model; the correlation coefficient (R^2) ranged from 0.997 to 0.999. This showed that the rate controlling step in adsorption process may be chemisorptions and *TC* adsorption occurs probably via van der Waals forces or ion exchange between the adsorbent and *TC* (Zhao *et al.* 2011; Wang *et al.* 2013). In addition, intraparticle diffusion model is
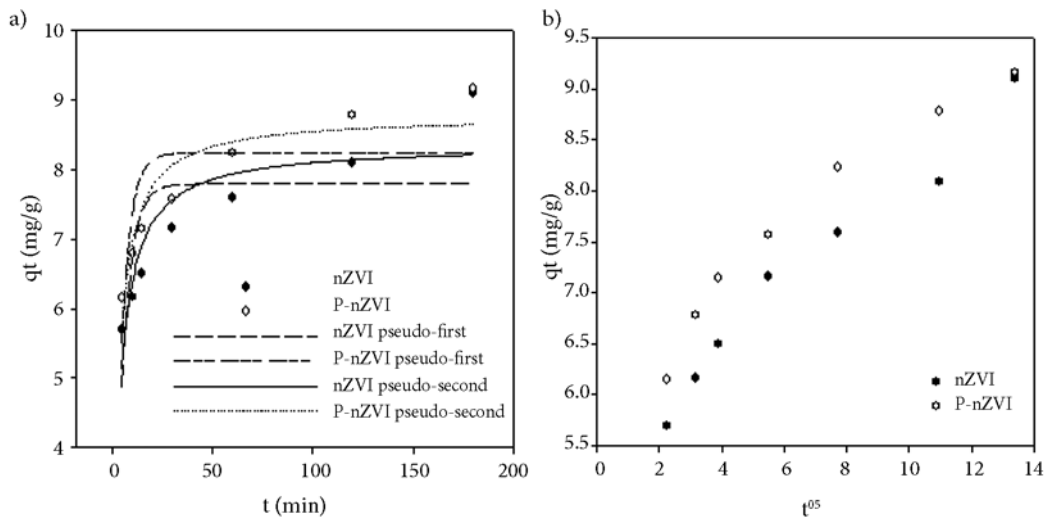
Fig. 8. Pseudo-first, pseudo-second order kinetic (a) and intra particle model (b) of *TC* onto nZVI and P-nZVI

Table 4. Adsorption kinetic parameters of the *TC* removal by the nZVI and P-nZVI

	Pseudo-first order			Pseudo-second order			Intra particle diffusion		
$q_{e,exp}$ (mg/g)	k_1 (min^{-1})	q_1 (mg/g)	R^2	k_2 (g·mg^{-1}min^{-1})	q_2 (mg/g)	R^2	k_i (mg/g·min$^{0.5}$)	C	R^2
nZVI									
9.10	0.198	7.79	0.728	0.038	8.35	0.900	0.277	5.33	0.984
P-nZVI									
9.16	0.221	8.23	0.768	0.043	8.77	0.937	0.253	5.99	0.975

not the one rate controlling step due to it was not linear (Guler, Sarioglu 2014; Ersoy *et al.* 2010). Therefore; *TC* adsorption was affected both intra particle diffusion and boundary diffusion.

2.4.2. Reduction kinetic

The pseudo-first-order kinetic model was used for *TC* removal by nZVI and P-nZVI. Pseudo-first-order kinetics is showed as below (Chen *et al.* 2013; Zhang 2003):

$$\ln\frac{[TC]_e}{[TC]_o} = -k_{obs}t \ ,　　　　(12)$$

where k_{obs}(min^{-1}) is the rate constant of a pseudo-first-order kinetic model (Table 5). The removal of *TC* by nZVI and P-nZVI composites fitted well to the pseudo-first order kinetic model. The k_{obs} decreased for nZVI and P-nZVI as the initial *TC* concentration increased from 25 to 300 mg/L, respectively. This indicated that the reduction of *TC* occurs at the interface of nZVI and P-nZVI (Chen *et al.* 2013; Shi *et al.* 2011). The rate of reduction was related to the active sites of adsorbent and the initial *TC* concentration (Chen *et al.* 2013). Moreover, the rate constants k_{obs} of P-nZVI were higher than nZVI. Pumice provided a mechanical supports and reactivity (Chen *et al.* 2013; Choi *et al.* 2009).

Table 5. k_{obs} for removal of *TC*

TC conc (mg/L)	k_{obs}(min^{-1})	R^2
25	0.012	0.902
50	0.007	0.959
nZVI　　100	0.002	0.952
200	0.001	0.861
300	0.002	0.943
25	0.018	0.972
50	0.008	0.964
P-nZVI　　100	0.004	0.963
200	0.002	0.974
300	0.004	0.982

2.5. Thermodynamic parameters

The standard free energy change (ΔG^o; kJ/mol), standart enthalpy change (ΔH^o; kJ/mol) and standart entropy change (ΔS^o; kJ/mol.K) were calculated using the following equations (Chen *et al.* 2013):

$$\Delta G^o = -RT\ln K_c \ ;　　　　(13)$$

$$\ln K_c = \frac{\Delta S^o}{R} - \frac{\Delta H^o}{RT} \ ,　　　　(14)$$

where *T* is the reaction temperature (Kelvin) and K_c is the q_e/C_e. ΔH^o and ΔS^o were determined from a plot of ln K_L versus 1/*T*. The thermodynamic parameters are listed in Table 6.

Table 6. Thermodynamic parameters obtained for *TC* removal onto nZVI and P-nZVI composites

	ΔH^o (kJ/mol)	ΔS^o (kJ/mol·K)	ΔG^o (kJ/mol)		
			298 K	308 K	318 K
nZVI	−2.87	52.84	−18.85	−18.82	−19.93
P-nZVI	−17.95	−0.51	−19.13	−17.44	−17.93

Negative values of ΔG^o and ΔH^o indicate that *TC* adsorption was spontaneous, feasible and exothermic. The negative value of ΔS showed that the adsorption process is due to an associative mechanism and decreased randomness. The negative ΔS value (−0.51 kJ/mol for P-nZVI) mean that the decreased randomness at the solid/liquid interface during adsorption.

2.6. Proposed mechanism for *TC* removal by nZVI and P-nZVI

The core and shell structure of nZVI composites provide two uptake mechanisms. The core is an electron source and can reduce ions, so it has a higher reduction potential than iron. The shell has hydroxyl groups and it provides uptake on the nZVI surface of adsorbate via surface complexation (Üzüm *et al.* 2009).

Based on the results presented here, possible mechanisms for *TC* removal from aqueous solutions involves (i) *TC* adsorption by nZVI and P-nZVI and (ii) *TC* reduction via oxidation of Fe^0 to Fe^{3+} (Li *et al.* 2012; Chen *et al.* 2013; Zhang *et al.* 2012). The yellow flocculent precipitates were observed, indicating that TC_xFe$_{(1-x)}$(OH)$_3$ complexes were formed. Similar results were reported by other researches (Chen *et al.* 2011). Possible reactions and mechanism are as follows (Eqs (15)–(19) and Fig. 9):

$$TC + nZVI \text{ or } P\text{-}nZVI \rightarrow TC\text{-}nZVI \text{ or}$$
$$TC\text{-}P\text{-}nZVI \text{ (adsorption);}　　　　(15)$$

$$TC + Fe^0 + 2H^+ \rightarrow Fe^{2+} + H_2 + TC + 2e^-$$
$$\text{(oxidation in acidic solution);}　　　(16)$$

$$TC + Fe^0 + 2H_2O \rightarrow Fe^{2+} + H_2 + 2OH^- + TC + 2e^-$$
$$\text{(oxidation in basic solution);}　　　(17)$$

$$TC + 2Fe^{2+} + 2H^+ + 1/2O_2 \rightarrow Fe^{3+} + TC + H_2O$$
$$\text{(oxidation in acidic solution);}　　　(18)$$

$$xTC + (1-x)Fe^{3+} + 3H_2O \rightarrow TC_x Fe_{(1-x)}(OH)_3 + 3H^+$$
$$\text{(reduction).}　　　(19)$$
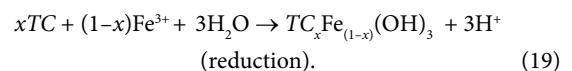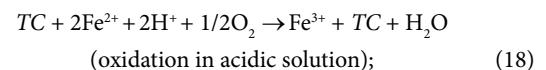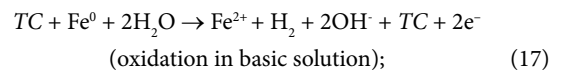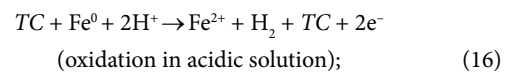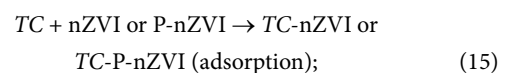
Conclusions

This study demonstrated that nZVI and P-nZVI composites can be used successfully used for *TC* removal in
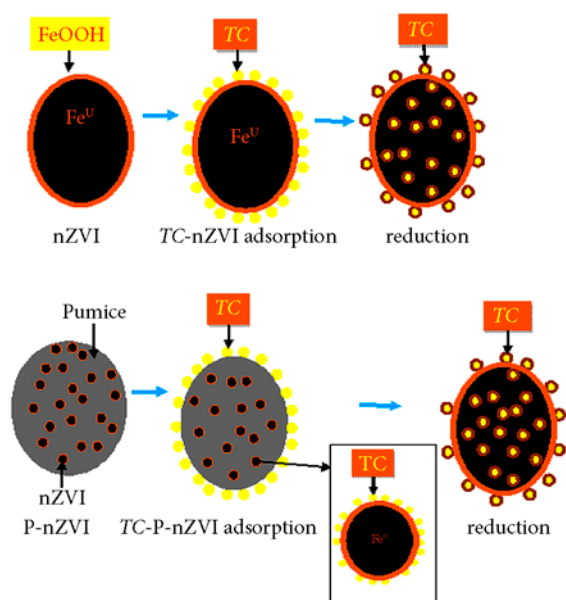
Fig. 9. Proposed mechanism for *TC* removal by nZVI and P-nZVI

aqueous solutions. Pumice was an effective support material as a dispersant and stabilizer that reduced nZVI aggregation. Mean pore diameters of nZVI and P-nZVI were 40 nm and 27 nm, respectively. pH significantly affects removal efficiency. FTIR, XRD, SEM and TEM analyses indicated that nZVI particles were dispersed on the surface of pumice and aggregation of nZVI was decreased. The removal of *TC* by nZVI and P-nZVI may comprise two processes: (i) reduction (ii) adsorption.

Finally, the high removal efficiency (91% and 92% for nZVI and P-nZVI, respectively) demonstrated that nZVI and P-nZVI are promising materials for treating pharmaceutical compounds in wastewaters.

Acknowledgements

References

Andrade, A. L.; Souza, D. M.; Pereira, M. C.; Fabris, J. D.; Domingues, R. Z. 2009. Synthesis and characterization of magnetic nanoparticles coated with silica through a sol–gel approach, *Ceramica* 55: 420–424. http://dx.doi.org/10.1590/S0366-69132009000400013

Asgari, G.; Roshani, B.; Ghanizadeh, G. 2012. The investigation of kinetic and isotherm of fluoride adsorption onto functionalize pumice stone, *Journal of Hazardous Materials* 17(218): 123–132. http://dx.doi.org/10.1016/j.jhazmat.2012.03.003

Boxall, A. B. A.; Kolpin, D. W.; SØrensen, B. H.; Tolls, J. 2003. Are veterinary medicines causing environmental risks?, *Environmental Science & Technolgy* 37: 286–294. http://dx.doi.org/10.1021/es032519b

Cao, J. S.; Zhang, W. X. 2006. Stabilization of chromium ore processing residue (COPR) with nanoscale iron particles, *Journal of Hazardous Materials* 132: 213–219. http://dx.doi.org/10.1016/j.jhazmat.2005.09.008

Chang, P. H.; Li, Z. H.; Yu, T. L.; Munkhbayer, S.; Kuo, T. H.; Hung, Y. C.; Jean, J. S.; Lin, K. H. 2009b. Sorptive removal of tetracycline from water by palygorskite, *Journal of Hazardous Materials* 165: 148–155. http://dx.doi.org/10.1016/j.jhazmat.2008.09.113

Chang, P. H.; Li, Z.; Jean, J. S.; Jiang, W. T.; Wang, C. J.; Lin, K. H. 2009a. Adsorption and intercalation of tetracycline by swelling clay minerals, *Applied Clay Science* 46: 27–36. http://dx.doi.org/10.1016/j.clay.2009.07.002

Chang, P. H.; Li, Z.; Jean, J. S.; Jiang, W. T.; Wang, C. J.; Lin, K. H. 2012. Adsorption of tetracycline on 2:1 layered non-swelling clay mineral illite, *Applied Clay Science* 67–68: 158–163. http://dx.doi.org/10.1016/j.clay.2011.11.004

Chen, H.; Luoa, H.; Lana, Y.; Donga, T.; Hub, B.; Wang, Y. 2011. Removal of tetracycline from aqueous solutions using polyvinylpyrrolidone (PVP-K30) modified nanoscale zero valent iron, *Journal of Hazardous Materials* 192: 44–53. http://dx.doi.org/10.1016/j.jhazmat.2011.04.089

Chen, Z.; Wang, T.; Jin, X.; Chen, Z.; Megharaj, M.; Naidu, R. 2013. Multifunctional kaolinite-supported nanoscale zerovalent iron used for the adsorption and degradation of crystal violet in aqueous solution, *Journal of Colloid Interface Science* 398: 59–66. http://dx.doi.org/10.1016/j.jcis.2013.02.020

Choi, H.; Al-Abed, S. R.; Agarwal, S. 2009. Catalytic role of palladium and relative reactivity of substituted chlorines during trapping and treatment of PCBs on reactive activated carbon, *Environmental Science & Technolgy* 43: 7510–7515. http://dx.doi.org/10.1021/es901298b

Cumbal, L.; Greenleaf, J.; Leun, D.; Sen-Gupta, A. K. 2003. Polymer supported inorganic nanoparticles: characterization and environmental applications, *Reactive & Functional Polymers* 54: 167–180. http://dx.doi.org/10.1016/S1381-5148(02)00192-X

Daughton, C. G.; Ternes, T. A. 1999. Pharmaceuticals and personal care products in the environment: agents of subtle change?, *Environmental Health Perspectives* 107: 907–938. http://dx.doi.org/10.1289/ehp.99107s6907

Dickinson, M.; Scott, T. B. 2010. The application of zero-valent iron nanoparticles for the remediation of a uranium-contaminated waste effluent, *Journal of Hazardous Materials* 178: 171–179. http://dx.doi.org/10.1016/j.jhazmat.2010.01.060

Ersoy, B.; Sariisik, A.; Dikmen, S.; Sariisik, G. 2010. Characterization of acidic pumice and determination of its electrokinetic properties in water, *Powder Technology* 197: 129–135. http://dx.doi.org/10.1016/j.powtec.2009.09.005

Fang, Z.; Chen, J.; Qiu, X.; Qiu, X.; Cheng, W.; Zhu, L. 2011. Effective removal of antibiotic metronidazole from water by nanoscale zero-valent iron particles, *Desalination* 268: 60–67. http://dx.doi.org/10.1016/j.desal.2010.09.051

Figueroa, R. A.; Leonard, A.; MacKay, A. A. 2004. Modeling tetracycline antibiotic sorption to clays, *Environmental Science & Technolgy* 38: 476–483. http://dx.doi.org/10.1021/es0342087

Gao, Y.; Li, Y.; Zhang, L.; Huang, H.; Hu, J.; Shah, S. M.; Su, X. 2012. Adsorption and removal of tetracycline antibiotics from aqueous solution by graphene oxide, *Journal of Colloid Interface Science* 368: 540–546. http://dx.doi.org/10.1016/j.jcis.2011.11.015

Guler, U. A.; Sarioglu, M. 2014. Removal of tetracycline from wastewater using pumice stone: equilibrium, kinetic and thermodynamic studies, *Journal of Environmental Health* 12: 79. http://dx.doi.org/10.1186/2052-336x-12-79

Kanel, S. R.; Greneche, J. M.; Choi, H. 2006. Arsenic (V) removal from groundwater using nanoscale zero-valent iron as a colloidal reactive barrier material, *Environmental Science & Technolgy* 40: 2045–2050. http://dx.doi.org/10.1021/es0520924

Kanel, S. R.; Manning, B.; Charlet, L.; Choi, H. 2005. Removal of arsenic (III) from groundwater by nanoscale zero-valent iron, *Environmental Science & Technolgy* 39: 1291–1298. http://dx.doi.org/10.1021/es048991u

Kim, S. A.; Kannan, S. K.; Lee, K. J.; Park, Y. J.; Shea, P. J.; Lee, W. H.; Ki, H. M.; Oh, B. T. 2013. Removal of Pb(II) from aqueous solution by a zeolite–nanoscale zero-valent iron composite, *Chemical Engineering Journal* 217: 54–60. http://dx.doi.org/10.1016/j.cej.2012.11.097

Kitis, M.; Kaplan, S. S.; Karakaya, E.; Yigit, N. O.; Civelekoglu, G. 2007. Adsorption of natural organic matter from waters by iron coated pumice, *Chemosphere* 66: 130–138. http://dx.doi.org/10.1016/j.chemosphere.2006.05.002

Li, Y.; Li, J.; Zhang, Y. 2012. Mechanism insights into enhanced Cr(VI) removal using nanoscale zerovalent iron supported on the pillared bentonite by macroscopic and spectroscopic studies, *Journal of Hazardous Materials* 227–228: 211–218. http://dx.doi.org/10.1016/j.jhazmat.2012.05.034

Li, Z.; Schulz, L.; Ackley, C.; Fenske, N. 2010. Adsorption of tetracycline on kaolinite with pH-dependent surface charges, *Journal of Colloid and Interface Science* 351: 254–260. http://dx.doi.org/10.1016/j.jcis.2010.07.034

Liu, T.; Wang, Z. L.; Yan, X.; Zhang, B. 2014. Removal of mercury (II) and chromium (VI) from wastewater using a new and effective composite: pumice-supported nanoscale zero-valent iron, *Chemical Engineering Journal* 245: 34–40. http://dx.doi.org/10.1016/j.cej.2014.02.011

Moraci, N.; Calabrò, P. S. 2010. Heavy metals removal and hydraulic performance in zero-valent iron/pumice permeable reactive barriers, *Journal of Environmental Management* 91: 2336–2341. http://dx.doi.org/10.1016/j.jenvman.2010.06.019

Shi, L. N.; Lin, Y. M.; Zhang, X.; Chen, Z. L. 2011. Synthesis, characterization and kinetics of bentonite supported nZVI for the removal of Cr (VI) from aqueous solution, *Chemical Engineering Journal* 171(2): 612–617. http://dx.doi.org/10.1016/j.cej.2011.04.038

Song, X.; Liu, D.; Zhang, G.; Frigon, M.; Meng, X.; Li, K. 2014. Adsorption mechanisms and the effect of oxytetracycline on activated sludge, *Bioresource Technology* 151: 428–431. http://dx.doi.org/10.1016/j.biortech.2013.10.055

Üzüm, Ç.; Shahwan, T.; Eroglu, A. E.; Hallam, K. R.; Scott, T. B.; Lieberwirth, I. 2009. Synthesis and characterization of kaolinite-supported zero-valent iron nanoparticles and their application for the removal of aqueous Cu^{2+} and Co^{2+} ions, *Applied Clay Science* 43: 172–181. http://dx.doi.org/10.1016/j.clay.2008.07.030

Wang, T.; Su, J.; Jina, X.; Chena, Z.; Megharaj, M.; Naidu, R. 2013. Functional clay supported bimetallic nZVI/Pd nanoparticles used for removal of methyl orange from aqueous solution, *Journal of Hazardous Materials* 262: 819–825. http://dx.doi.org/10.1016/j.jhazmat.2013.09.028

Wang, W.; Jin, Z.; Li, T.; Zhang, H.; Gao, S. 2006. Preparation of spherical iron nanoclusters in ethanol–water solution for nitrate removal, *Chemosphere* 65: 1396–1404. http://dx.doi.org/10.1016/j.chemosphere.2006.03.075

Xu, X. R.; Li, X. Y. 2010. Sorption and desorption of antibiotic tetracycline on marine sediments, *Chemosphere* 78: 430–436. http://dx.doi.org/10.1016/j.chemosphere.2009.10.045

Yuan, P.; Fan, M.; Yang, D.; He, H.; Liu, D.; Yuan, A.; Zhu, J.; Chen, T. 2009. Montmorillonite-supported magnetite nanoparticles for the removal of hexavalent chromium Cr(VI) from aqueous solutions, *Journal of Hazardous Materials* 166: 821–829. http://dx.doi.org/10.1016/j.jhazmat.2008.11.083

Zhang, D.; Niu, H.; Zhang, X.; Meng, Z.; Cai, Y. 2011a. Strong adsorption of chlorotetracyline on magnetite nanoparticles, *Journal of Hazardous Materials* 92: 1088–1093. http://dx.doi.org/10.1016/j.jhazmat.2011.06.015

Zhang, W. 2003. Nanoscale iron particles for environmental remediation: an overview, *Journal of Nanoparticle Research* 5: 323–332. http://dx.doi.org/10.1023/A:1025520116015

Zhang, X.; Lin, S.; Chen, Z.; Megharaj, M.; Naidu, R. 2011c. Kaolinite-supported nanoscale zero-valent iron for removal of Pb^{2+} from aqueous solution: reactivity, characterization and mechanism, *Water Research* 45: 3481–3488. http://dx.doi.org/10.1016/j.watres.2011.04.010

Zhang, X.; Lin, S.; Lu, X. Q.; Chen, Z. I. 2010. Removal of Pb (II) from water using synthesized kaolin supported nanoscale zero-valent iron, *Chemical Engineering Journal* 163: 243–248. http://dx.doi.org/10.1016/j.cej.2010.07.056

Zhang, Y.; Li, Y.; Li, J.; Hu, L.; Zheng, X. 2011b. Enhanced removal of nitrate by a novel composite: nanoscale zero valent iron supported on pillared clay, *Chemical Engineering Journal* 171: 526–531. http://dx.doi.org/10.1016/j.cej.2011.04.022

Zhang, Y.; Li, Y.; Zheng, X. 2011d. Removal of atrazine by nanoscale zero valent iron supported on organobentonite, *Science of the Total Environment* 409: 625–630. http://dx.doi.org/10.1016/j.scitotenv.2010.10.015

Zhao, Y.; Geng, J.; Wang, X.; Gu, X.; Gao, S. 2011. Adsorption of tetracycline onto goethite in the presence of metal cations and humic substances, *Journal of Colloid and Interface Science* 361: 247–251. http://dx.doi.org/10.1016/j.jcis.2011.05.051

Zhao, Y.; Gu, X.; Gao, S.; Geng, J.; Wang. X. 2012. Adsorption of tetracycline (TC) onto montmorillonite: cations and humic acid effects, *Geoderma* 183–184: 12–18. http://dx.doi.org/10.1016/j.geoderma.2012.03.004

Ulker Asli GULER. Doctor of Environmental Science (2010). Ass. Prof. Dr of Environmental Engineering Department of Cumhuriyet University. Research interest: wastewater treatment, adsorption/biosorption, environmental technologies.